REPORT NO.
UCB/SEMM-88/17

STRUCTURAL ENGINEERING
MECHANICS AND MATERIALS

VIBRATION ANALYSIS OF FLUID-SOLID SYSTEMS USING A FINITE ELEMENT DISPLACEMENT FORMULATION

BY

HARN C. CHEN and ROBERT L. TAYLOR

SEPTEMBER 1988

DEPARTMENT OF CIVIL ENGINEERING
UNIVERSITY OF CALIFORNIA
BERKELEY, CALIFORNIA

Vibration Analysis of Fluid-Solid Systems Using a Finite Element Displacement Formulation

Harn C. Chen and Robert L. Taylor

Department of Civil Engineering

University of California, Berkeley

Abstract

This report presents a finite element solution for the vibration interaction between an inviscid fluid and a solid. The equation of motion governing the inviscid fluid is expressed in terms of the displacements. This ensures that compatibility and equilibrium will be satisfied automatically along the interface of the coupled systems. To suppress circulation modes with non-zero energy, reduced integration is used when computing the element *stiffness* matrix contributed by the fluid. In addition, a projection is used on the element mass matrix in order to remove the spurious modes which result from the use of reduced integration. Numerical examples for both fluid and coupled fluid-solid systems are performed and the results are shown.

Contents

This research was sponsored by the Lawrence Livermore National Laboratory under contract CERDA LLNL-1513603. This support and the interest of Dr. G. L. Goudreau are gratefully acknowledged.

1. Introduction

Fluid-solid interactions arise in many engineering problems. Predicting the response of fluid-solid coupled systems is generally a difficult task. In most practical problems, it is not possible to obtain closed form analytical solutions for the coupled systems. As a result, much effort has gone into the development of general finite element methods for coupled systems. Some difficulties, however, have been encountered in using the finite element method to predict the dynamic responses of coupled systems. The goal of this study is to develop a robust method suitable for finding the natural frequencies and mode shapes of coupled systems.

The vibration analysis of fluids alone is usually treated by choosing the pressure as the primary variable, as in [Petyt *et al*; Kiefling and Feng]. For coupled systems, however, there are generally two approaches in terms of the variables used. One is to use either the pressure alone or the displacements alone as variables, as described in [Tabarrok]. The other is to use both the pressure and the displacements as variables, as shown in [Zienkiewicz and Bettess, Olson and Bathe]. In finite element analysis, displacements are predominantly used to describe the motion of solids. Therefore, using a displacement formulation to describe fluids has the advantage that no special interface consideration is required. That is, the compatibility and equilibrium along the interface between solids and fluids will be satisfied automatically and boundary conditions can be easily taken into account. Moreover, the finite element matrices contributed by fluids can be generated from an existing finite element code for solids and there is no need to develop a new code for fluids. For these reasons, it is popular to use the displacement formulation for fluids when dealing with coupled problems [Maheri].

It has been found that the displacement formulation for fluids suffers from the presence of circulation modes. These circulation modes may have zero frequencies as well as non-zero frequency, depending upon the type of element and mesh used. Consequently it is not possible to separate the real modes from the circulation modes by merely inspecting the values of the frequencies computed. To deal with the difficulty due to the circulation modes, an irrotational constraint can be introduced and taken into account by a penalty method [Hamdi *et al*]. The circulation modes can then be identified by changing the

value of the penalty parameter. Reduced integration can be used, together with the irrotational constraint, to construct the stiffness matrix for better results [Wilson and Khalvati]. Both methods require solving the problem more than once using different penalty values and often require trial-and-error methods to determine an optimum value for the irrotational constraint parameter.

In this study, we derive a finite element displacement formulation for a fluid and show its similarity to that for a solid. To suppress the circulation modes which have non-zero frequencies, we use reduced integration to find the stiffness contributed by the fluid. The use of reduced integration, unfortunately, leads to element stiffness matrices which are rank-deficient and thus produces extra zero-energy modes [Bicanic and Hinton]. These extra zero-energy modes can combine with circulation modes into global modes which have the same frequency as the real modes, thus corrupting the mode shapes of the real modes. To remove these spurious modes, we first identity the extra zero-energy modes at the element level. This is accomplished by splitting the strain and subsequently the stiffness matrices into two parts using the 4-node element shape function representation given in [Belytschko and Bachrach]. Then, we remove these extra zero-energy modes from the solution space by performing a projection on the element mass matrix. In this way, we can use the reduced-integration technique without introducing the spurious modes into the solution. Finally, numerical examples are solved and results are presented to show the performance of the under-integrated stiffness matrix and the projected mass matrix in treating fluids and coupled problems.

2. Governing Equations for Inviscid Fluid

We consider an ideal inviscid barotropic fluid. The governing equations for small amplitude motions of such fluid are given by

$$p_{,i} + \rho \dot{v}_i = 0 \tag{2.1}$$

$$\dot{p} + \rho c^2 v_{k,k} = 0 \tag{2.2}$$

where v_i is the velocity components, ρ is the mass density, p is the pressure, and c is the acoustic speed in the fluid. In this formulation two set of variables, the velocity and the

pressure, are used to describe the behavior of the fluid.

It is possible to combine (2.1) and (2.2) to obtain a single-variable formulation for the fluid. Since only small amplitude motions are considered, the velocity in the fluid can be taken as

$$v_i = \dot{u}_i \tag{2.3}$$

where u_i is the displacement components. After differentiating (2.2) with respect to t and (2.1) with respect to x_i, one can subtract (2.1) from (2.2) to obtain the classical wave equation

$$\ddot{p} - c^2 p_{,ii} = 0 \tag{2.4}$$

where only the pressure is used as variable. However, the solid is described generally in terms of the displacements. Therefore, when dealing with coupled systems where a pressure formulation is used to describe the fluid, additional effort is required in order to completely satisfy equilibrium and compatibility along the interface between the fluid and the solid.

An alternative single-variable formulation can be obtained in the following way. Substituting (2.3) into (2.2) and then integrating with respect to t leads to

$$p = -\rho c^2 u_{k,k} \tag{2.5}$$

Differentiating (2.5) with respect to x_i and then substituting the result into (2.1), we obtain

$$\rho \ddot{u}_i - \rho c^2 u_{k,ki} = 0 \tag{2.6}$$

where only the displacements are used as variables. If this displacement formulation is used to describe the fluid in coupled systems, then compatibility and equilibrium will be automatically satisfied along the interface between the fluid and the solid.

The weak form of equation (2.6) is

$$\int_\Omega w_i \left(\rho \ddot{u}_i - \rho c^2 u_{k,ki} \right) d\Omega = 0 \tag{2.7}$$

Performing integration by parts on the second term, one obtains

$$\int_\Omega w_i \rho \ddot{u}_i + \int_\Omega w_{i,i} \rho c^2 u_{k,k} d\Omega = \int_\Gamma w_i \rho c^2 u_{k,k} n_i d\Gamma \tag{2.8}$$

The right hand side in the above is zero along rigid boundaries since the weighting

function w_i must satisfy the condition of $w_i\, n_i = 0$ on the boundary Γ_u. Therefore, the weak form of eqn (2.6) becomes

$$\int_\Omega [\, w_i\, \rho\, \ddot{u}_i + w_{i,i}\, \rho\, c^2\, u_{k,k}\,]\, d\Omega = -\int_{\Gamma_\sigma} w_i\, n_i\, \bar{p}\, d\Gamma \tag{2.9}$$

where $\bar{p}$ is a known pressure.

Using the usual finite element discretization procedure for a two dimensional problem, one can express the trial functions $\mathbf{u} = [\, u_1, u_2\,]^t$ and the the weighting functions $\mathbf{w} = [\, w_1, w_2\,]^t$ as

$$\mathbf{u} \approx \bar{\mathbf{N}}\, \mathbf{U} \qquad \mathbf{w} \approx \bar{\mathbf{N}}\, \mathbf{W}$$

where the $\bar{\mathbf{N}}$ is a shape function array which relates the displacements $\mathbf{u}$ and $\mathbf{w}$ to the nodal displacements $\mathbf{U}$ and $\mathbf{W}$. For convenience in subsequent discussion, we introduce a differential operator

$$\mathbf{L} = \begin{bmatrix} \dfrac{\partial}{\partial x_1} & \dfrac{\partial}{\partial x_2} \end{bmatrix} \tag{2.10}$$

so that the divergence of the displacement vector can be written as

$$u_{i,i} = \mathbf{L}\, \mathbf{u} = \mathbf{L}\, \bar{\mathbf{N}}\, \mathbf{U} = \mathbf{B}\, \mathbf{U} \tag{2.11}$$

Using the above notation, we have

$$w_i\, \ddot{u}_i = \mathbf{w}^t\, \ddot{\mathbf{u}} = \mathbf{W}\, \bar{\mathbf{N}}^t\, \bar{\mathbf{N}}\ddot{\mathbf{U}} \tag{2.12}$$

and

$$w_{i,i}\, u_{k,k} = \mathbf{W}^t\, \mathbf{B}^t\, \mathbf{B}\, \mathbf{U} \tag{2.13}$$

and the governing equation (2.9) then becomes

$$\mathbf{W}^t \int_\Omega [\, \bar{\mathbf{N}}^t\, \rho\, \bar{\mathbf{N}}\, \ddot{\mathbf{U}} + \mathbf{B}^t\, \rho\, c^2\, \mathbf{B}\, \mathbf{U}\,]\, d\Omega = -\mathbf{W}^t \int_{\Gamma_\sigma} \bar{\mathbf{N}}^t\, \mathbf{n}\, \bar{p}\, d\Gamma \tag{2.14}$$

This is true for all $\mathbf{W}$, therefore we have the matrix equation :

$$\mathbf{M}\, \ddot{\mathbf{U}} + \mathbf{K}\, \mathbf{U} = \mathbf{F} \tag{2.15}$$

where the coefficient matrices $\mathbf{M}$ and $\mathbf{K}$ given by

$$\mathbf{M} = \int_\Omega \rho\, \bar{\mathbf{N}}^t\, \bar{\mathbf{N}}\, d\Omega \tag{2.16a}$$

$$\mathbf{K} = \int_{\Omega} \rho\, c^2\, \mathbf{B}^t\, \mathbf{B}\, d\Omega \tag{2.16b}$$

$$\mathbf{F} = -\int_{\Gamma_e} \bar{\mathbf{N}}^t\, \mathbf{n}\, \bar{p}\, d\Gamma \tag{2.16c}$$

Equation (2.15) is the same as that which appears in the vibration analysis of elastic solid systems. Therefore, one can directly assemble the stiffness and mass matrices due to the solid part and those due to the fluid part together to obtain the final matrices for the whole coupled system. In addition, the **K** in (2.15) is equal to the volumetric part of the stiffness matrix for a two-dimensional elasticity problem. Therefore, by choosing appropriate material constants, an existing finite element code for the two-dimensional elasticity problem can readily be used to compute the element mass and stiffness matrix for the fluid element.

In the following sections we show results from using reduced integration to compute the stiffness matrix and how to construct a projected mass matrix to eliminate the problems introduced by the reduced integration.

3. Under-integrated Stiffness Matrix

Consider a general 4-node quadrilateral element with constant unit thickness. The shape functions, N_I, for the 4-node bilinear element are given by

$$N_I(\xi\,,\,\eta) = \frac{1}{4}\,(1 + \xi_I\,\xi)\,(1 + \eta_I\,\eta) \tag{3.1}$$

where ξ_I and η_I are values of the natural coordinates ξ and η at the node I. For convenience, we can express the shape functions in vector form as

$$\mathbf{N}(\xi,\,\eta) = (\mathbf{1} + \xi\,\mathbf{s} + \eta\mathbf{t} + \xi\,\eta\,\mathbf{h}) \tag{3.2}$$

where

$$\mathbf{s} = \frac{1}{4}\,[\,-1,\,1,\,1,\,-1\,]^t, \qquad \mathbf{t} = \frac{1}{4}\,[\,-1,\,-1,\,1,\,1\,]^t,$$

$$\mathbf{1} = \frac{1}{4}\,[\,1,\,1,\,1,\,1\,]^t, \qquad \mathbf{h} = \frac{1}{4}\,[\,1,\,-1,\,1,\,-1\,]^t. \tag{3.3}$$

We note that any one of the above four vectors is orthogonal to the other three vectors. Therefore, they can be used as a basis in $\mathbb{R}^4$. This orthogonality will be useful in

subsequent derivations.

The coordinates of a point in the element can be expressed by

$$x = \mathbf{x}^t \mathbf{N} \qquad y = \mathbf{y}^t \mathbf{N} \tag{3.4}$$

where $\mathbf{x}$ and $\mathbf{y}$ contain the x-coordinates and y-coordinates of the 4 nodes respectively.

The Jacobian of the transformation between the global coordinate $x-y$ and local coordinate $\xi-\eta$ is expressed by

$$\mathbf{J} = \begin{bmatrix} \frac{\partial x}{\partial \xi} & \frac{\partial y}{\partial \xi} \\ \frac{\partial x}{\partial \eta} & \frac{\partial y}{\partial \eta} \end{bmatrix} = \begin{bmatrix} J_{11} & J_{12} \\ J_{21} & J_{22} \end{bmatrix} \tag{3.5}$$

The expressions in eqns (3.4) and (3.2) may be used to define the coefficients in the Jacobian matrix. The result is

$$\begin{aligned} J_{11} &= \mathbf{x}^t \mathbf{s} + \mathbf{x}^t \mathbf{h}\,\eta \qquad & J_{12} &= \mathbf{y}^t \mathbf{s} + \mathbf{y}^t \mathbf{h}\,\eta \\ J_{21} &= \mathbf{x}^t \mathbf{t} + \mathbf{x}^t \mathbf{h}\,\xi \qquad & J_{22} &= \mathbf{y}^t \mathbf{t} + \mathbf{y}^t \mathbf{h}\,\xi \end{aligned} \tag{3.6}$$

The determinant of the Jacobian can be expressed by

$$\det \mathbf{J} = J(\xi, \eta) = J_0 + J_1 \xi + J_2 \eta \tag{3.7}$$

where the values of J_0, J_1, and J_2 can be shown to be

$$\begin{aligned} J_0 &= \mathbf{x}^t \mathbf{s}\, \mathbf{y}^t \mathbf{t} - \mathbf{x}^t \mathbf{t}\, \mathbf{y}^t \mathbf{s} \\ J_1 &= \mathbf{x}^t \mathbf{s}\, \mathbf{y}^t \mathbf{h} - \mathbf{x}^t \mathbf{h}\, \mathbf{y}^t \mathbf{s} \\ J_2 &= \mathbf{x}^t \mathbf{h}\, \mathbf{y}^t \mathbf{t} - \mathbf{x}^t \mathbf{t}\, \mathbf{y}^t \mathbf{h} \end{aligned} \tag{3.8}$$

It is useful to note that J_1 and J_2 are zero when the element is a parallelogram and J_0 is equal to one-fourth of the area A of the element. The inverse of the Jacobian is expressed by

$$\mathbf{J}^{-1} = \begin{bmatrix} \frac{\partial \xi}{\partial x} & \frac{\partial \eta}{\partial x} \\ \frac{\partial \xi}{\partial y} & \frac{\partial \eta}{\partial y} \end{bmatrix} = \frac{1}{J} \begin{bmatrix} J_{22} & -J_{12} \\ -J_{21} & J_{11} \end{bmatrix} \tag{3.9}$$

Based upon (3.4), the displacement approximations for an isoparametric element are given by

$$u_1 = \mathbf{U}_1^t \mathbf{N} \qquad u_2 = \mathbf{U}_2^t \mathbf{N} \tag{3.10}$$

where $\mathbf{U}_1$ and $\mathbf{U}_2$ contain the nodal values of u_1 and u_2 respectively. Alternatively, as shown by Belytschko *et. al.* [6], the displacement approximations may be written as

$$\begin{aligned} u_1 &= \mathbf{U}_1^t (\Delta + x\,\mathbf{b}_x + y\,\mathbf{b}_y + h\,\boldsymbol{\gamma}) \\ u_2 &= \mathbf{U}_2^t (\Delta + x\,\mathbf{b}_x + y\,\mathbf{b}_y + h\,\boldsymbol{\gamma}) \end{aligned} \tag{3.11}$$

where

$$\Delta = [\,\mathbf{1} - \mathbf{x}^t\mathbf{1}\,\mathbf{b}_x - \mathbf{y}^t\mathbf{1}\,\mathbf{b}_y\,] \tag{3.12a}$$

$$\boldsymbol{\gamma} = [\,\mathbf{h} - \mathbf{x}^t\mathbf{h}\,\mathbf{b}_x - \mathbf{y}^t\mathbf{h}\,\mathbf{b}_y\,] \tag{3.12b}$$

and

$$h = \xi\eta \tag{3.12c}$$

with

$$\mathbf{b}_x = \frac{\partial \mathbf{N}}{\partial x}\Big|_{\xi=\eta=0} \tag{3.12d}$$

$$\mathbf{b}_y = \frac{\partial \mathbf{N}}{\partial y}\Big|_{\xi=\eta=0} \tag{3.12e}$$

which can be shown to be

$$\mathbf{b}_x = \frac{1}{J_0}(\,\mathbf{s}\mathbf{y}^t\mathbf{t} - \mathbf{t}\mathbf{y}^t\mathbf{s}\,) \tag{3.12d}$$

$$\mathbf{b}_y = \frac{1}{J_0}(\,\mathbf{t}\mathbf{x}^t\mathbf{s} - \mathbf{s}\mathbf{x}^t\mathbf{t}\,) \tag{3.12e}$$

This form will be particularly useful in subsequent calculations where derivatives of the functions are involved.

To form the stiffness matrix, we first compute the **B** matrix. From (2.11) we have

$$\mathbf{B} = \begin{bmatrix} \dfrac{\partial}{\partial x_1} & \dfrac{\partial}{\partial x_2} \end{bmatrix} \begin{bmatrix} \mathbf{N}^t & \mathbf{0}^t \\ \mathbf{0}^t & \mathbf{N}^t \end{bmatrix} = \begin{bmatrix} \mathbf{N}^t_{,x} & \mathbf{N}^t_{,y} \end{bmatrix} \tag{3.13}$$

Using (3.11) we can split the **B** into two parts :

$$\mathbf{B} = \mathbf{B}_0 + \mathbf{B}_1 \tag{3.14}$$

where the first part results from the derivatives of the first three terms in (3.11), namely,

$$\mathbf{B}_0 = \begin{bmatrix} \mathbf{b}_x^t & \mathbf{b}_y^t \end{bmatrix} \tag{3.15}$$

which is *constant* over the element. The second part results from the derivatives of the h term and is given by

$$\mathbf{B}_1 = \begin{bmatrix} h_{,x}\,\boldsymbol{\gamma}^t & h_{,y}\,\boldsymbol{\gamma}^t \end{bmatrix} = \mathbf{g}\,\Gamma \tag{3.16}$$

with

$$\Gamma = \begin{bmatrix} \boldsymbol{\gamma}^t & \mathbf{0}^t \\ \mathbf{0}^t & \boldsymbol{\gamma}^t \end{bmatrix} \qquad \in \mathbb{R}^{2\times 8} \tag{3.17}$$

and

$$\mathbf{g} = \begin{bmatrix} h_{,x} & h_{,y} \end{bmatrix} \qquad \in \mathbb{R}^{1\times 2} \tag{3.18}$$

The partial derivatives of h are given by

$$\begin{Bmatrix} \dfrac{\partial h}{\partial x} \\ \dfrac{\partial h}{\partial y} \end{Bmatrix} = \begin{bmatrix} \dfrac{\partial \xi}{\partial x} & \dfrac{\partial \eta}{\partial x} \\ \dfrac{\partial \xi}{\partial y} & \dfrac{\partial \eta}{\partial y} \end{bmatrix} \begin{Bmatrix} \eta \\ \xi \end{Bmatrix} \tag{3.19}$$

This can be computed using (3.9) and (3.6) to give

$$\begin{Bmatrix} \dfrac{\partial h}{\partial x} \\ \dfrac{\partial h}{\partial y} \end{Bmatrix} = \frac{1}{J} \begin{Bmatrix} \mathbf{y}^t\,\mathbf{t}\,\eta - \mathbf{y}^t\,\mathbf{s}\,\xi \\ \mathbf{x}^t\,\mathbf{s}\,\xi - \mathbf{x}^t\,\mathbf{t}\,\eta \end{Bmatrix} \tag{3.20}$$

Accordingly, we may observe that the integrals of the derivatives of h have the property

$$\int_\Omega h_{,x}\,d\Omega = 0 \qquad \int_\Omega h_{,y}\,d\Omega = 0 \tag{3.21}$$

This holds on any quadrilateral element and is called an *orthogonality* property.

The element stiffness matrix is given by (2.15b). Using the split of the **B** given by (3.14), we can write the element stiffness matrix given by (2.15b) as

$$\mathbf{K} = \int_{\Omega} \rho\, c^2 \left[\mathbf{B}_0^t \mathbf{B}_0 + \mathbf{B}_0^t \mathbf{B}_1 + \mathbf{B}_1^t \mathbf{B}_0 + \mathbf{B}_1^t \mathbf{B}_1 \right] d\Omega \tag{3.22}$$

In the above the integrals of products between $\mathbf{B}_0$ and $\mathbf{B}_1$ vanish due to the orthogonality property, i.e. (3.21). Thus, the stiffness matrix reduces to

$$\mathbf{K} = \int_{\Omega} \rho\, c^2\, \mathbf{B}_0^t \mathbf{B}_0\, d\Omega + \int_{\Omega} \rho\, c^2\, \mathbf{B}_1^t \mathbf{B}_1\, d\Omega = \mathbf{K}_0 + \mathbf{K}_1 \tag{3.23}$$

Since $\mathbf{B}_0$ is constant over the element, we have

$$\mathbf{K}_0 = \rho\, c^2 A\, \mathbf{B}_0^t \mathbf{B}_0 \tag{3.24}$$

where A is the area of the element. It is apparent that a one-point Gaussian quadrature is enough to compute the $\mathbf{K}_0$ exactly. Using (3.16) the $\mathbf{K}_1$ matrix may be written as

$$\mathbf{K}_1 = \int_{\Omega} \rho\, c^2\, \mathbf{B}_1^t \mathbf{B}_1\, d\Omega = \Gamma^t \mathbf{W}\, \Gamma \tag{3.25}$$

The 2×2 matrix $\mathbf{W}$ may be easily computed to be

$$\mathbf{W} = \int_{\Omega} \mathbf{g}^t \mathbf{g}\, d\Omega = \begin{bmatrix} H_{xx} & H_{xy} \\ H_{xy} & H_{yy} \end{bmatrix} \tag{3.26}$$

where

$$H_{xx} = \int_{\Omega} h_{,x}^2\, d\Omega\,, \quad H_{yy} = \int_{\Omega} h_{,y}^2\, d\Omega\,, \quad H_{xy} = \int_{\Omega} h_{,x} h_{,y}\, d\Omega \tag{3.27}$$

It is important to note that the H_{xx}, H_{xy}, and H_{yy} are all equal to zero if they are evaluated by 1-point Gaussian quadrature. Therefore, $\mathbf{K}_0$ is what will be obtained if the element stiffness matrix is under-integrated, i.e. integrated using 1-point Gaussian quadrature. Here, the $\mathbf{K}_1$ can be looked upon as a correction to give a fully integrated element stiffness.

4. Projected Mass Matrix

In the previous section we split the matrix $\mathbf{B}$ into two parts, $\mathbf{B}_0$ and $\mathbf{B}_1$ and accordingly the stiffness $\mathbf{K}$ into two parts, $\mathbf{K}_0$ and $\mathbf{K}_1$. The important fact is that $\mathbf{K}_0$ is actually what will be obtained when the stiffness is under-integrated. A direct calculation of the eigenvalues of a 4-node element can verify that the rank of $\mathbf{K}_0$ is less than the rank of $\mathbf{K}$

by two. We first identify the modes which have zero energy when the $\mathbf{K}$ is under-integrated so that we know what is to be tackled. To this end, we can use the four vectors in (3.3) to construct the following eight element displacement modes $\mathbf{d}_i$ for $i = 1, \ldots, 8$, where

$$\mathbf{d}_1 = \begin{bmatrix} 1 \\ 0 \end{bmatrix} \quad \mathbf{d}_2 = \begin{bmatrix} 0 \\ 1 \end{bmatrix} \quad \mathbf{d}_3 = \begin{bmatrix} s \\ 0 \end{bmatrix} \quad \mathbf{d}_4 = \begin{bmatrix} 0 \\ s \end{bmatrix}$$

$$\mathbf{d}_5 = \begin{bmatrix} t \\ 0 \end{bmatrix} \quad \mathbf{d}_6 = \begin{bmatrix} 0 \\ t \end{bmatrix} \quad \mathbf{d}_7 = \begin{bmatrix} h \\ 0 \end{bmatrix} \quad \mathbf{d}_8 = \begin{bmatrix} 0 \\ h \end{bmatrix} \tag{4.1}$$

They represent, respectively, rigid body, uniform extension, shear, and hourglass modes in the x and y directions for the 4-node element. These eight modes are linearly independent since they satisfy the condition

$$\mathbf{d}_i^t \, \mathbf{d}_j = \frac{1}{4} \delta_{ij} \qquad i, j = 1, \ldots, 8 \tag{4.2}$$

where δ_{ij} is the Kronecker delta. Therefore, They can be used as a set of basis vectors for the 8-dimensional solution space of the element and any solution can be simply written as a linear combination of these eight modes. With these basis modes defined, we note that

$$\mathbf{B}_0 \mathbf{d}_7 = \mathbf{0} \qquad \mathbf{B}_0 \mathbf{d}_8 = \mathbf{0} \tag{4.3}$$

while $\mathbf{B}_1 \mathbf{d}_7$ and $\mathbf{B}_1 \mathbf{d}_8$ are not equal to zero. Therefore, it can be concluded that the hourglass modes $\mathbf{d}_7$ and $\mathbf{d}_8$, or equivalently any linear combination of them, are the two extra zero-energy modes when the under-integrated stiffness matrix $\mathbf{K}_0$ is used. These two modes can combine with other modes and result in *global modes* which have nonzero energy but are spurious.

To prevent the presence of the spurious modes in the computation, we can remove the subspace *span* $\{\mathbf{d}_7, \mathbf{d}_8\}$ from the solution space of the element. That is, we construct a subspace Q

$$\mathbf{Q} = \mathbf{I} - \alpha_7 \mathbf{d}_7 \mathbf{d}_7^t - \alpha_8 \mathbf{d}_8 \mathbf{d}_8^t \qquad \in \mathbb{R}^{8\times 8} \tag{4.4}$$

where

$$\alpha_k = \frac{1}{\mathbf{d}_k^t \mathbf{d}_k} = 4 \qquad k = 7, 8 \tag{4.5}$$

and then form the projection of the element consistent mass matrix onto this subspace‡ :

$$\mathbf{M}_0 = \mathbf{Q}^t \, \mathbf{M} \, \mathbf{Q} \tag{4.6}$$

A direct calculation can show that the projected element mass matrix $\mathbf{M}_0$ has the property that the generalized masses for the two extra zero-energy modes, and therefore any linear combination of them, are zero, i. e.,

$$\mathbf{d}_i^t \, \mathbf{M}_0 \, \mathbf{d}_i = 0 \qquad i = 7, 8 \tag{4.7}$$

while the generalized masses for the other modes, and therefore any linear combination of them, are preserved, i. e.,

$$\mathbf{d}_j^t \, \mathbf{M}_0 \, \mathbf{d}_j = \mathbf{d}_j^t \, \mathbf{M} \, \mathbf{d}_j \qquad j = 1, \ldots, 6 \tag{4.8}$$

Therefore, by projecting the element mass matrix onto the subspace $\mathbf{Q}$ we make *span* $\{\mathbf{d}_7, \mathbf{d}_8\}$ become the null space of the element mass matrix so that they will not be present in the computation. In this way, we are able to remove the spurious modes due to the under-integration of the element stiffness matrix, as will be shown by examples in the next section.

5 Numerical Examples

The method of using the under-integrated stiffness matrix and projected mass matrix described above for the fluid were tested by solving some example problems. We first solve a simple problem with known solution to illustrate the effect of using the under-integrated stiffness matrix and projected mass matrix. We then study the convergence property of the method presented here by gradually changing the size of the mesh. We also show the effect of the interaction between fluid and solid by comparing the frequencies of the coupled system and the frequencies of the solid alone and of the fluid alone. Finally, we vary some properties of the fluid to study how the frequencies of the solid are affected.

---

‡ The projected mass $\mathbf{M}_0$ cannot be transformed to diagonal form and satisfy the properties on the subspace.

Fluid in a rigid cavity

The frequencies of a fluid in a rigid cavity are computed. The dimension of the cavity is 20 by 20, the density ρ of the fluid is 1 and the acoustic speed a is 340. Table 1 presents the frequencies obtained using : (I) fully-integrated stiffness $\mathbf{K}$ and conventional mass $\mathbf{M}$, (II) under-integrated stiffness $\mathbf{K}_0$ and conventional mass $\mathbf{M}$, and (III) under-integrated stiffness $\mathbf{K}_0$ and projected mass $\mathbf{M}_0$. By comparing with the analytic solution and plotting the mode shapes found, we find the following. In (I), there are only 4 real modes and all the others are spurious modes. In (II), there are 8 spurious modes with zero frequency, three real modes, and five spurious modes with non-zero frequency. In (III), the first 8 are spurious modes with zero frequency and all the other 8 are real modes.

From these results, we can draw the following conclusions: First, some of the solutions from using the $\mathbf{K}$ are real modes, however, there is no simple way to distinguish them from the circulation modes. Second, the use of reduced integration makes the frequencies of all the circulation modes zero so that one can identify them merely by inspection. Unfortunately, there still exist modes which have multiplicity more than 2. even though the frequencies of these modes are good approximates to the analytic solutions. From the analytic solutions, we know that only two of these modes with high multiplicity can be real modes and the redundant ones are spurious. In the computation, however, the mode shapes of the real modes are corrupted by the redundant modes. Therefore, all these modes should not be considered as real modes in practice. Finally, by using the $\mathbf{M}_0$, we can suppress the spurious modes and therefore remove the redundant modes from the solutions. Figure 1 shows the real modes obtained using (III).

Mesh sensitivity

We can investigate the effect of the size of the mesh on the error for the frequencies of fluid in cavity. For a rectangular plane cavity $a \times b$ confined by perfectly rigid walls, the frequencies ω are given by the analytic solution :

$$\omega_{(m,n)} = c\ \pi\ [\ (\frac{n}{a})^2 + (\frac{m}{b})^2\ ]^{1/2}$$

where m, n are integers and c is the acoustic speed in the fluid. Here the error is defined

by

$$\text{error } (\%) = \frac{\text{numerical solution} - \text{analytic solution}}{\text{analytic solution}} \times 100$$

Figure 2 shows the errors on the lower frequencies versus the number n of divisions along the sides. A skew 5×5 mesh, as shown in Figure 3, is also tested and the errors are 1.62% for (1,0) mode, 0.23% for (1,1) mode, 6.55% for (2,0) mode, 3.33% for (2,1) mode, and -0.09% for (2,2) mode. The errors from the skew 5×5 mesh are about the same level as the errors from the regular 5×5 mesh. These results show that satisfactory results can be obtained by using a rather coarse mesh and the convergence rate is quadratic.

Coupled system

The difficulty of using the displacement formulation to analyze the fluid can be resolved by employing simultaneously the under-integrated stiffness matrix and the projected mass matrix. This method is now applied to a coupled system to investigate the interaction between the fluid and the solid. We solve the same cavity example as above, but one wall of the cavity is now replaced by a simply supported elastic plate while the other three walls remain rigid. The material properties for the plate are : plate bending rigidity D is 10^8, thickness is 1, and density is 1. For this plane strain problem, we may use a beam element to model the plate element by choosing the beam bending rigidity equal to the plate bending rigidity D. The same coarse mesh as above is used and there are only three plate elements. To illustrate the effect of interaction, we show in Table 2 the frequencies of the coupled system, of the plate alone, and of the fluid alone in a rigid cavity. By plotting the mode shapes, we can identify whether a mode is associated with the plate or with the fluid. For the modes associated with the plate, the presence of the fluid affects the bending modes, but does not affect the axial and rotational modes. For the modes associated with the fluid, the normal modes in one direction is greatly affected due to the presence of the elastic plate, while the normal modes in the other direction and the tangential modes are almost unaffected.

Effect of coupling

We can investigate the effect of coupling by gradually changing some properties of the coupled system. For example, Table 3 presents the frequencies of the plate bending modes in the coupled system for different values of acoustic speed. These results are obtained using an uniform 5×5 mesh. From the Table 3 it is seen that the effect of coupling is most important on the fundamental mode of the plate. The fundamental mode of the plate always requires a compressibility for the fluid inside the cavity, so this frequency is strongly influenced as the compressibility of fluid increases. On the other hand, the higher modes are less affected by the compressibility of the fluid since their shapes occurs with little or no overall volume change in the fluid. To see this phenomenon, we present in Table 4 the frequencies of the plate bending modes for different values of fluid density. Increasing the density of the fluid will increase both the stiffness and mass of the fluid. We note that the increase in the stiffness has more effect on the fundamental mode due to the compressibility requirement and hence its frequency increases. On the other hand, the increase in the mass has more effect on the higher modes and thus reduces the frequencies of those modes. For comparison, we show in Figure 4 the first few modes of the fluid alone in the cavity, in Figure 5 the fluid modes, and in Figure 6 the plate modes of the coupled system.

6 Conclusions

A simple finite element displacement method is presented for the vibration analysis of fluid-solid coupled systems. The main feature is to use an under-integrated stiffness matrix and a projected mass matrix for the fluid. Due to the use of the displacement formulation, no special consideration is required for the interface of coupled systems and existing finite element programs for the analysis of solids can be easily modified for the analysis of fluids and coupled systems. In contrast to the previously published displacement methods, the current method is straight forward and can suppress the spurious modes which have non-zero frequencies.

References

1. T. Belytschko and W.E. Bachrach, 'Efficient implementation of quadrilaterals with high coarse-mesh accuracy', *Computer Methods in Applied Mechanics and Engineering*, Vol. 54, 279-301 (1986).
2. N. Bicanic and E. Hinton, 'Spurious Modes in Two-Dimensional Isoparametric Elements', *Int J. num. Meth. Engng.*, **14**, 1545-1557 (1979).
3. M. A. Hamdi, Y. Ousset, and G. Verchery, 'A Displacement Method for the Analysis of Vibrations of Coupled Fluid-Structure Systems', *Int J. num. Meth. Engng.*, **13**, 139-150 (1978).
4. L. Kiefling and G. C. Feng, 'Fluid-Structure Finite Element Vibrational Analysis', *AIAA J.*, **14**, 2, 199-203 (1976).
5. M. R. Maheri, C. A. Taylor, and A. Blakeborough, 'Comparative Numerical Studies of Hydrodynamic Effects on Dam Structures', *Proceedings of the 8th European Conference on Earthquake Engineering*, Lisbon, 6.8/25-6.8/32 (1986).
6. L. Olson and K. Bathe, 'Analysis of Fluid-Structure Interactions. An Direct Symmetric Coupled Formulation Based on the Fluid Velocity Potential', *Computers and Structures*, **21**, 21-32 (1985).
7. M. Petyt, J. Lea and G. H. Koopmann, 'A Finite Element Method for Determining the Acoustic Modes of Irregular Shaped Cavities', *J. of Sound and Vibration*, **45**(4), 495-502 (1976).
8. B. Tabarrok, 'Dual Formulation for Acousto-Structural Vibrations', *Int J. num. Meth. Engng.*, **13**, 197-201 (1978).
9. E. L. Wilson and M. Khalvati, 'Finite Elements for the Dynamic Analysis of Fluid-Solid Systems', *Int J. num. Meth. Engng.*, **19**, 1657-1668 (1983).
10. O. C. Zienkiewicz and P. Bettess, 'Fluid-Structure Dynamic Interaction and Wave Forces. An Introduction to Numerical Treatment', *Int J. num. Meth. Engng.*, **13**, 1-16 (1978).
11. O. C. Zienkiewicz, *The Finite Element Method,* 3rd edn., McGraw-Hill, London, 1977.

Table 1

Results from different methods

K and **M**	mode	$\mathbf{K_0}$ and **M**	mode	$\mathbf{K_0}$ and $\mathbf{M_0}$	mode
7.667	*	0.000	*	0.000	*
39.504	*	0.000	*	0.000	*
39.504	*	0.000	*	0.000	*
55.868	*	0.000	*	0.000	*
55.868	*	0.000	*	0.000	*
55.868	*	0.000	*	0.000	*
55.868	*	0.000	*	0.000	*
77.008	(1,1)	0.000	*	0.000	*
88.335	*	55.868	(1,0)	55.868	(1,0)
124.924	*	55.868	(0,1)	55.868	(0,1)
124.924	*	74.954	(1,1)	75.332	(1,1)
124.924	*	124.924	*	124.924	(2,0)
124.924	*	124.924	*	124.924	(0,2)
131.021	(2,1)	124.924	*	128.169	(2,1)
131.021	(1,2)	124.924	*	128.169	(1,2)
153.000	(2,2)	124.924	*	144.250	(2,2)

* : spurious mode

Table 2

Comparison of frequencies of different systems

plate alone	fluid in cavity	coupled system	mode description
	0.000	0.000	spurious
	0.000	0.000	spurious
	0.000	0.000	spurious
	0.000	0.000	spurious
	0.000	0.000	spurious
	0.000	0.000	spurious
	0.000	0.000	spurious
	0.000	0.000	spurious
	55.868	52.103	(1,0)
	55.868	55.823	(0,1)
	75.332	75.200	(1,1)
	124.924	112.996	(2,0)
	124.924	124.924	(0,2)
	128.169	127.820	(2,1)
	128.169	127.940	(1,2)
	144.250	142.392	(2,2)
246.940		193.221	bending
998.626		775.046	bending
1643.168		1643.168	axial
2464.752		2464.752	rotational
3674.235		3674.235	axial
4583.023		3952.920	bending and rotational
8200.376		7055.985	bending and rotational
11294.910		11294.910	rotational

Table 3

frequencies of plate bending modes for different sound speed

acoustic speed	1st mode	2nd mode	3rd mode	4th mode
0	171.9	733.4	1821.5	3668.4
340	278.7	747.3	1825.6	3669.2
680	536.7	797.6	1838.3	3671.5
1020	802.3	916.3	1861.5	3675.5
1360	1068.4	1123.5	1899.2	3681.3

Table 4

frequencies of plate bending modes for different fluid density

density	1st mode	2nd mode	3rd mode	4th mode
0	246.8	988.6	2238.3	4038.8
1	278.7	747.3	1825.6	3669.2
10	285.0	394.4	923.1	2238.6
100	285.9	298.9	393.6	837.7
1000	285.9	289.4	315.2	347.4

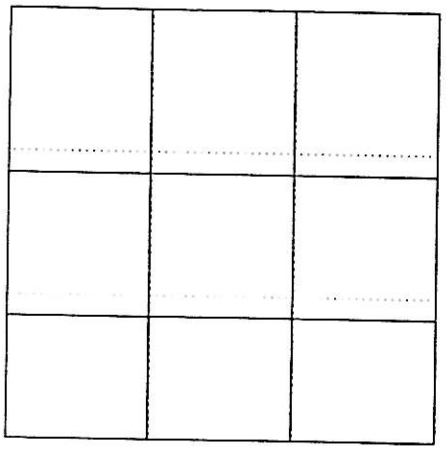

(1,0)

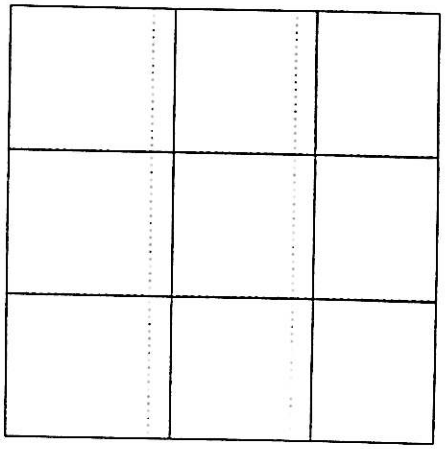

(0,1)

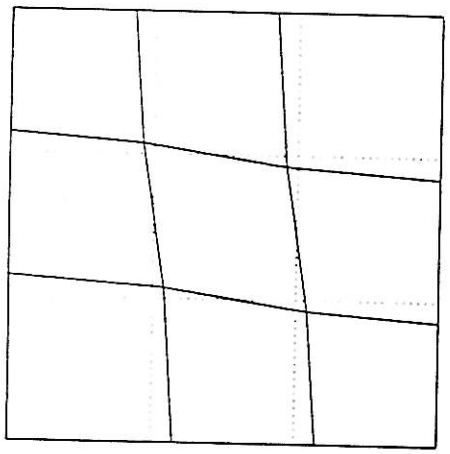

(1,1)

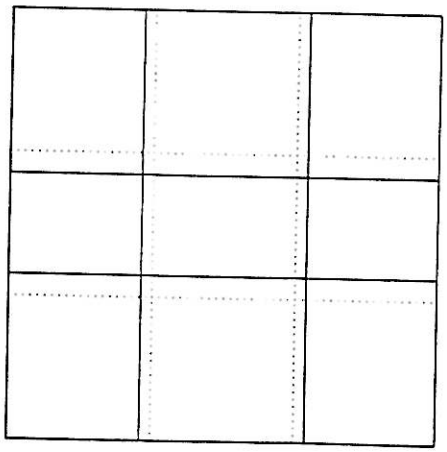

(2,0)

Figure 1 Mode shapes of fluid in cavity

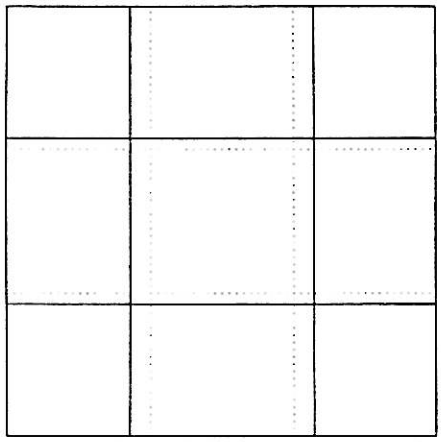

(0,2)

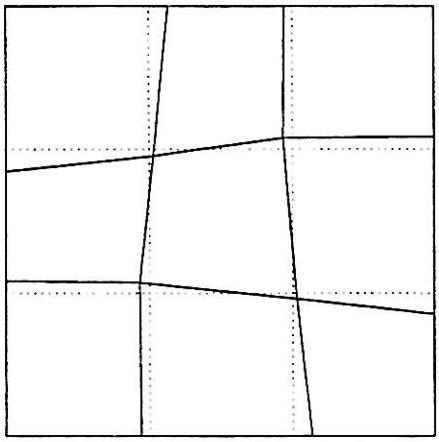

(2,1)

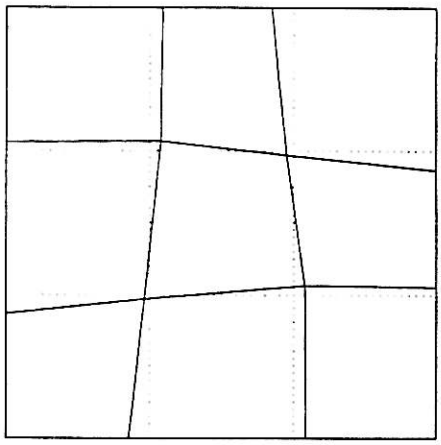

(1,2)

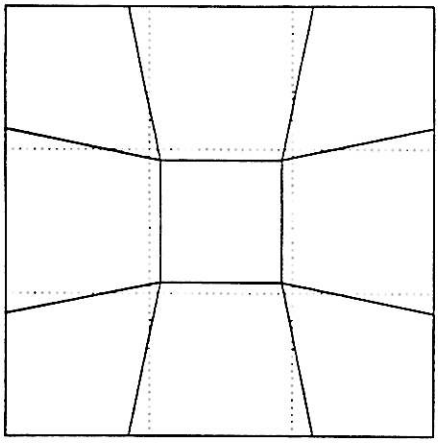

(2,2)

Figure 1 Mode shapes of fluid in cavity

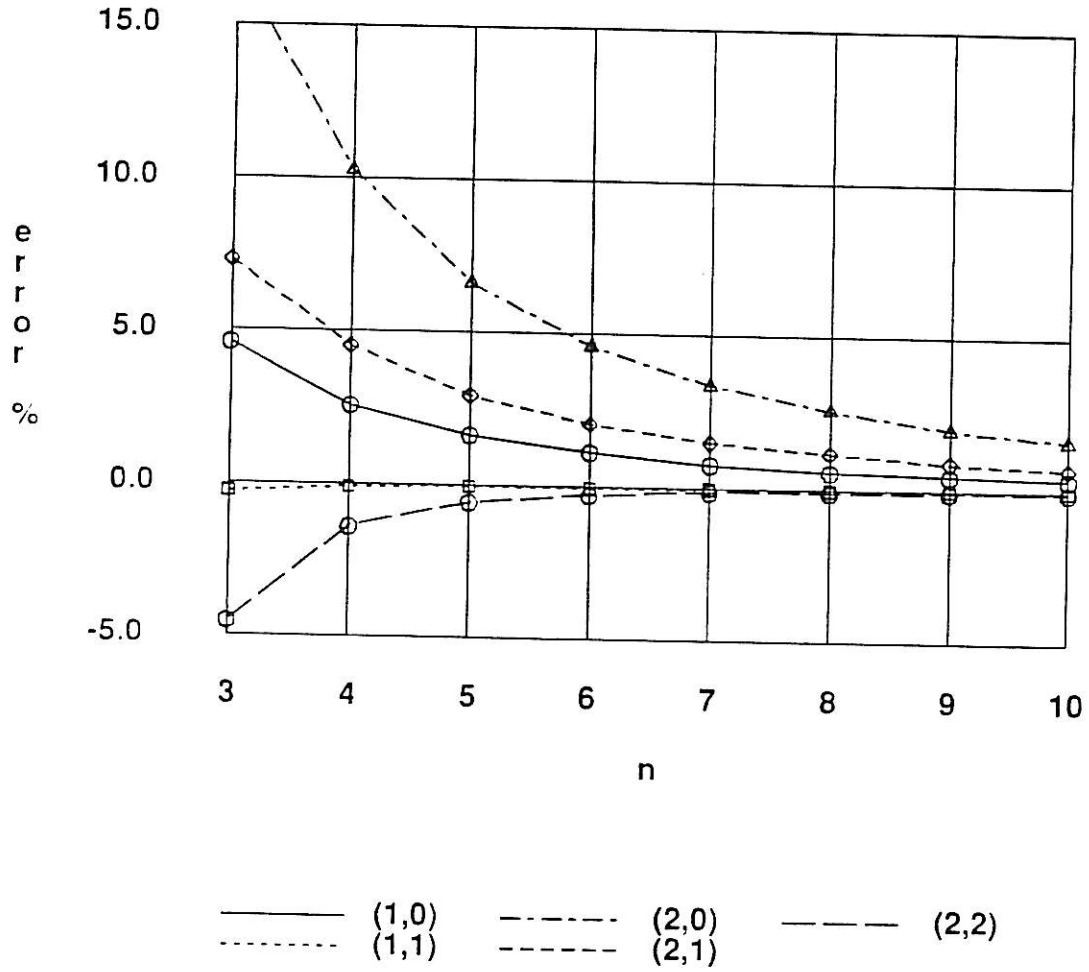

Figure 2 Error on frequencies versus number of divisions

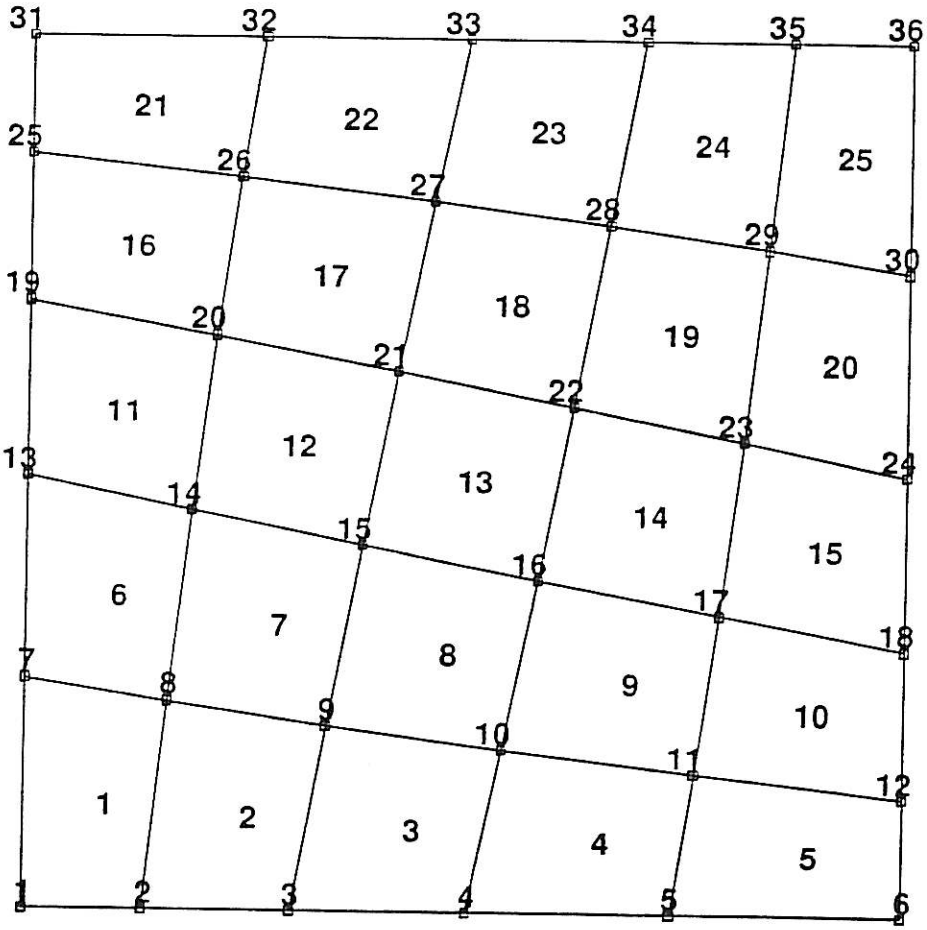

Figure 3 A skew 5 by 5 mesh

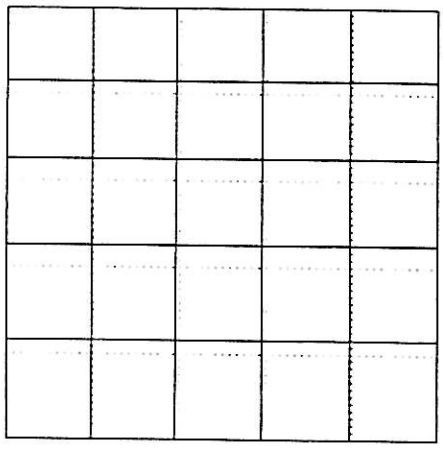

(1,0)

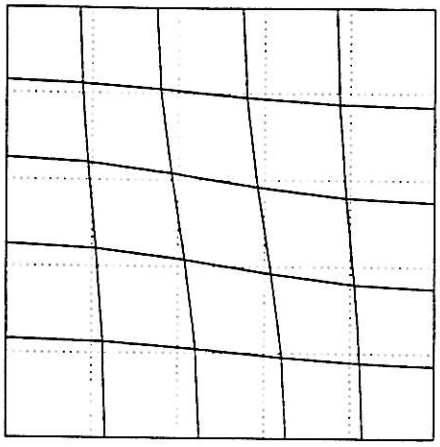

(1,1)

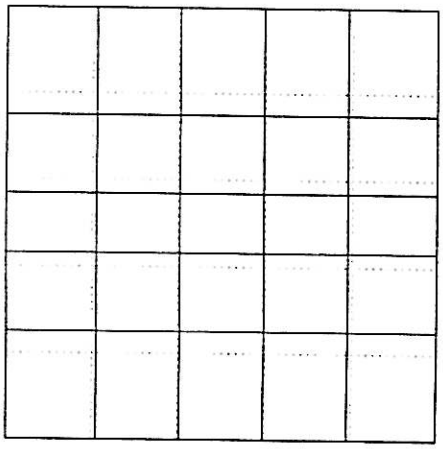

(2,0)

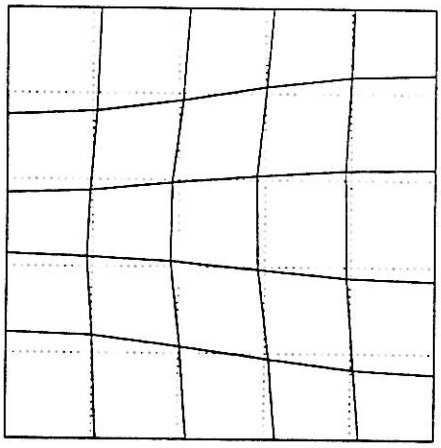

(2,1)

Figure 4 Modes of fluid in cavity

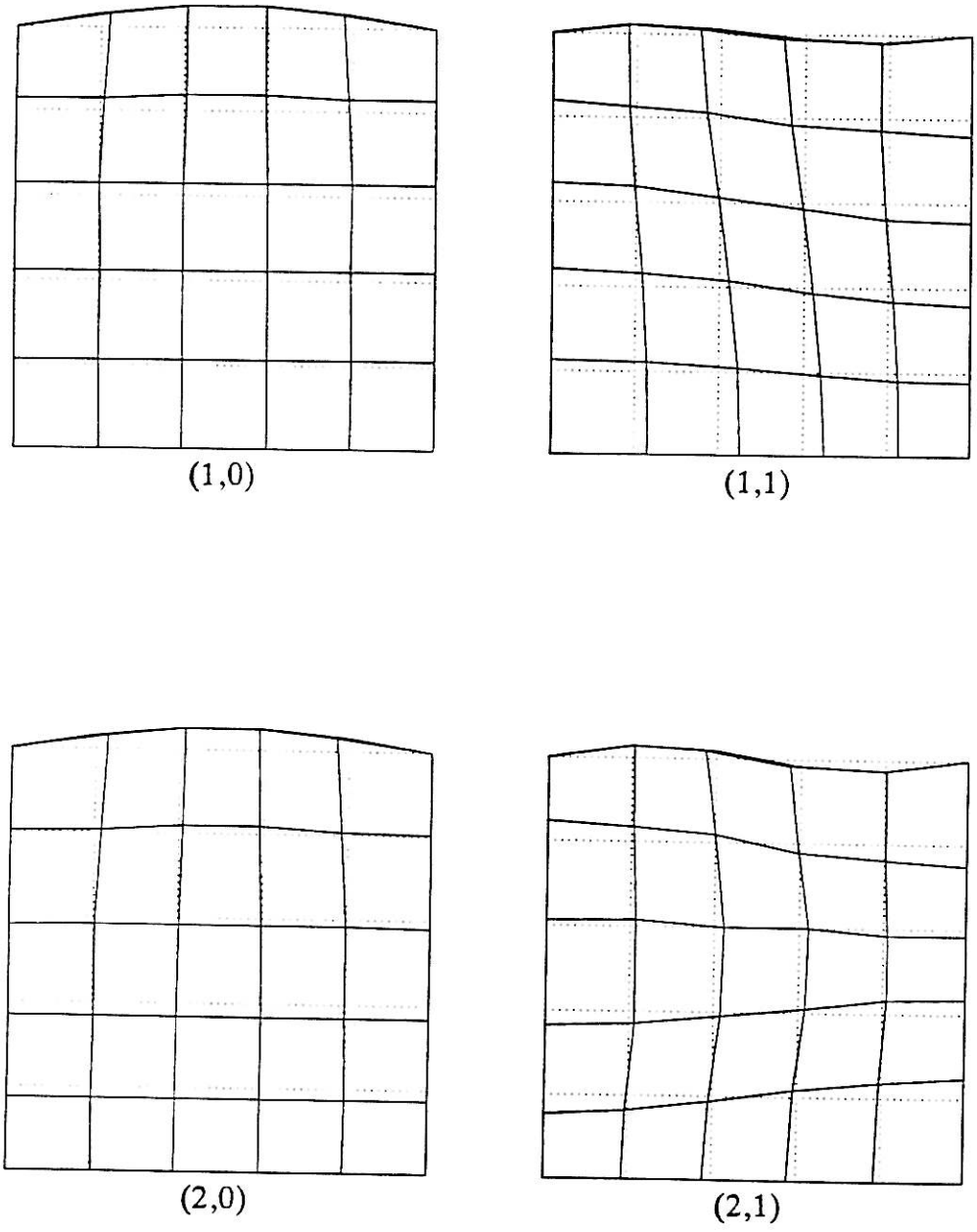

Figure 5 Fluid modes of coupled system

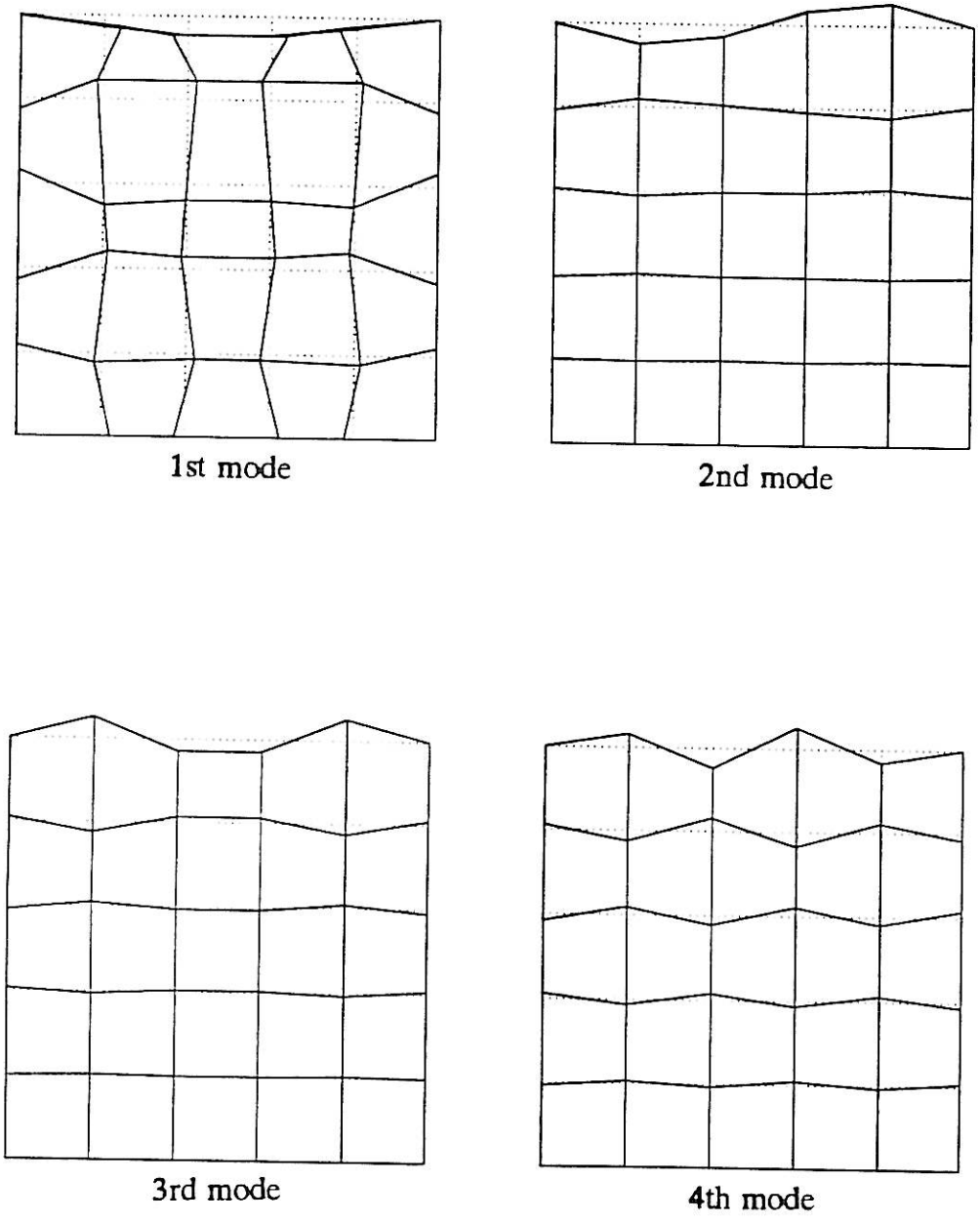

Figure 6 Plate modes of coupled system